Dry Contact Transfer Printing of Aligned Carbon Nanotube Patterns and Characterization of Their Optical Properties for Diameter Distribution and Alignment

Cary L. Pint,[†,⊥] Ya-Qiong Xu,[¶] Sharief Moghazy,[⊥] Tonya Cherukuri,[‡,⊥] Noe T. Alvarez,[‡,⊥] Erik H. Haroz,[†,⊥] Salma Mahzooni,[⊥] Stephen K. Doorn,[#] Junichiro Kono,[§,⊥] Matteo Pasquali,[‡,∥,⊥] and Robert H. Hauge[‡,⊥,*]

[†]Department of Physics and Astronomy, [‡]Department of Chemistry, [§]Department of Electrical and Computer Engineering, [∥]and Department of Chemical and Biomolecular Engineering, [⊥]The Richard E. Smalley Institute for Nanoscale Science and Technology, Rice University, Houston, Texas 77005, [¶]Department of Electrical Engineering and Computer Science and Department of Physics and Astronomy, Vanderbilt University, Nashville, Tennessee 37235, and [#]Chemistry Division, Los Alamos National Laboratory, Los Alamos, New Mexico 87545

ABSTRACT A scalable and facile approach is demonstrated where as-grown patterns of well-aligned structures composed of single-walled carbon nanotubes (SWNT) synthesized *via* water-assisted chemical vapor deposition (CVD) can be transferred, or printed, to any host surface in a single dry, room-temperature step using the growth substrate as a stamp. We demonstrate compatibility of this process with multiple transfers for large-scale device and specifically tailored pattern fabrication. Utilizing this transfer approach, anisotropic optical properties of the SWNT films are probed *via* polarized absorption, Raman, and photoluminescence spectroscopies. Using a simple model to describe optical transitions in the large SWNT species present in the aligned samples, polarized absorption data are demonstrated as an effective tool for accurate assignment of the diameter distribution from broad absorption features located in the infrared. This can be performed on either well-aligned samples or unaligned doped samples, allowing simple and rapid feedback of the SWNT diameter distribution that can be challenging and time-consuming to obtain in other optical methods. Furthermore, we discuss challenges in accurately characterizing alignment in structures of long *versus* short carbon nanotubes through optical techniques, where SWNT length makes a difference in the information obtained in such measurements. This work provides new insight to the efficient transfer and optical properties of an emerging class of long, large diameter SWNT species typically produced in the CVD process.

KEYWORDS: carbon nanotubes · carpets · optical absorption · Raman spectroscopy

One of the key topics of growing interest has been the integration of nanomaterials into devices and applications to replace or enhance the performance of conventional bulk materials. For many promising nanomaterials, including carbon nanotubes (CNTs), major progress in synthetic techniques has led to new challenges in processing as-synthesized nanomaterials in bulk with nanoscale precision in self-assembly or transfer to an optimal geometry for device applications. In this spirit, there has been a substantial effort to develop techniques of "soft lithography" to transfer a variety of nanoscale materials from one surface to another, including proteins,[1] nano- and microscale semiconducting materials,[2,3] and thin layers of carbon nanotubes,[4−9] typically utilizing stamps of polydimethylsiloxane (PDMS). When this is combined with horizontally aligned CNT growth processes,[10] transferred structures allow precision in the positioning of nanometer scale features for large-scale electronic device applications currently being realized.[11,12]

On another front, there has also been an evolving interest in the ability to grow single-walled carbon nanotubes (SWNT) from solid surfaces in arrays using chemical vapor deposition (CVD)[13,14] and specifically water-assisted SWNT growth,[15−17] where the arrays are oriented perpendicular to the growth substrate. The major feature limiting the large-scale application of this promising technique is the ability to retain the attractive features of the aligned array while transferring to a surface suitable for device applications. Recently, major progress in the ability to draw aligned thin films directly from CNT vertical arrays has enabled many exciting new CNT applications including loudspeakers,[18] incandescent displays,[19] and high-resolution TEM grids,[20] among others.[21−26] Undoubtedly, more flexibility in the transfer process for as-grown aligned films of long carbon nanotubes can enable substantially more routes for innovative

*Address correspondence to hauge@rice.edu.

Received for review September 30, 2009 and accepted January 14, 2010.

Published online January 21, 2010.
10.1021/nn9013356

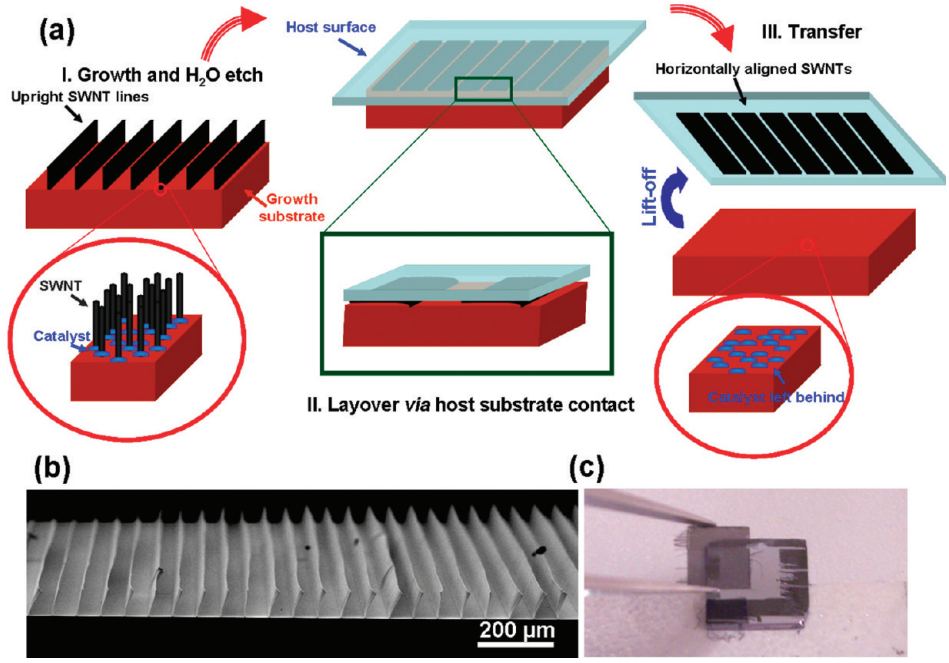

Figure 1. (a) Scheme depicting the process for dry contact transfer of aligned SWNTs as described in the text. (b) SEM image of an upright patterned growth prior to transfer, and (c) picture showing a complete transfer to a 5 mm × 5 mm wide diamond window.

device and application design. Recently, SWNT films transferred *via* the technique discussed in this work have been demonstrated to act as perfect linear polarizers for terahertz radiation.[21]

In addition to simple techniques for transfer of the aligned SWNT structures, another unique feature of CVD-grown SWNTs, and supergrowth SWNTs in particular, is the substantially larger and broader diameter distribution of SWNTs compared to those produced in processes such as HiPco or CoMoCat.[22] This makes common ensemble techniques developed to study the small diameter ($d < 1.5$ nm) SWNT species, such as visible and near-infrared (IR) fluorescence, absorption, and Raman characterization, insufficient to properly assess the majority population and features of the SWNT species in CVD-grown SWNTs with larger diameters and broad distributions. For these species, the spectral range is shifted into the infrared (IR) for the strongest interband transitions, and enhanced overlap of spectral features from individual (*n*,*m*) species makes specific nanotube assignment tedious and perhaps impossible without specifically designed samples. However, this represents a problem since there has been a dramatic increase in the prospect for applications made from aligned carbon nanotubes grown in CVD, and this will likely continue to increase. Therefore, it is important to accurately assess the composition and properties of the nanotubes (quality, alignment, *etc.*) from an ensemble perspective and evolve toward spectroscopic techniques that can be performed in resonance with the majority population of the SWNTs when working with such materials.

In this work, we first outline an efficient technique to transfer well-aligned films of semitransparent, pristine, and long (>25 μm) nanotubes grown *via* water-assisted CVD to optical windows. We further utilize polarized IR absorption to characterize broad envelopes describing collections of SWNT interband transitions that can allow a simple and relatively accurate assessment of the diameter distribution of nanotubes present in an aligned or unaligned sample. Finally, we compare the polarization dependence observed in the IR to that found in other spectroscopic techniques to emphasize the factors contributing to the anisotropy and considerations one should make when assigning properties based on SWNT alignment.

RESULTS AND DISCUSSION

Dry Transfer of Patterned, Aligned SWNTs. Analogous to the mechanism which guides a gecko to navigate along a surface normal to the plane of gravity, the transfer process for pristine, aligned SWNT films described here is a completely dry process that operates on the principle that van der Waals interaction between a layer of SWNTs and any host surface is greater than the van der Waals interaction and bond strength of the nanotubes to the growth substrate. This principle is the key as to why patterned, aligned CNTs have been demonstrated as effective adhesive tapes.[35,36] We demonstrate here that this mechanism can also be adapted to a transfer process yielding catalyst-free patterns of aligned carbon nanotubes on any arbitrary surface, with the nanotubes aligned in a direction parallel to the surface plane. The general steps of this transfer process are illustrated in Figure 1a. The first step involves the growth

of vertically aligned SWNT arrays in narrow line patterns, further illustrated in the scanning electron microscope (SEM) image shown in Figure 1b. To achieve this, optical lithography is utilized to define wafer-scale patterns of lines, where 10 nm of Al_2O_3 and 0.5 nm of Fe are deposited *via* e-beam deposition. Growth is then carried out through water-assisted CVD, and the result is an array of upright line structures of variable width and height, based on the lithographic pattern and reactor exposure time, respectively. The next step is a post-growth H_2/H_2O vapor etch which acts to release chemical bonds between catalyst particles and the nanotubes, leaving the interface between the grown nanotubes and the catalyst layer controlled by weaker van der Waals interactions. This step was a subject of a recent study[33] in which we focused on the transfer of short, homogeneous carpet films and marginally discussed the transfer of the line structures in a similar manner. Specifically, the transfer process using patterned SWNT arrays operates under the same general concept, but the transfer efficiency is optimized compared to homogeneous carpet materials since the aligned SWNT structures can be "toppled" over to achieve optimal van der Waals interaction between the edge of the SWNT line and the host surface. The transfer occurs since there will always be more surface area of the line exposed to interaction with the host (transfer) surface than the growth substrate since the line is toppled over while interacting with the host surface. As a result, the patterned SWNT can be easily lifted away as the catalyst remains on the clean growth substrate that is left behind. In our experience, we find few constraints on surfaces effective for transfer, as transfers to surfaces ranging in surface roughness (*i.e.*, tpx or commercially available polymers with microscale roughness), surface potential, and cleanliness routinely exhibited clean transfer. However, in extreme cases of surface roughness of contamination, we foresee the transfer process to be adversely affected, even though we have not investigated this extensively. Shown in Figure 1c is a photograph of a transfer from a typical growth substrate to a 5 mm $\times$ 5 mm diamond window (0.5 mm thick). From this photograph, it is evident that the diamond window (initially transparent) is uniformly coated with a thin film of SWNT from the growth surface, which visually confirms the clean footprint from the diamond window. In addition, one can also observe that some SWNT lines protrude from the edge of the diamond, indicating that the line structures have detached and are quite free of interaction with the growth substrate. A key feature in achieving the best transfer with this process is fine-tuning the amount of time in which the SWNT arrays are exposed to the H_2/H_2O etch.[33] Typically, the optimal time in our experiments ranges between 3 and 4 min, even though this varies with the growth conditions. In the limit of long exposure to the H_2/H_2O etch (typically greater than 10 min), the lines are found to spontaneously detach in the growth reactor and be lost to the vacuum pump. Although this detachment is mostly attributed to H_2O etching of C in the presence of a catalyst, we also speculate that Ostwald ripening of the catalyst particles in the growth environment may also play a role.[37]

The primary benefit of this technique, in comparison to other established processes for transfer, is that the process is performed completely in the dry state with only a single step. Compared to the range of "soft lithographic" techniques that exist, this process is quicker, less destructive, and is scalable to large areas (wafer-scale). However, it is geared toward the fabrication of SWNT array structures that are substantially thicker compared to those obtained *via* horizontally aligned growth on single-crystal surfaces, where an intermediate PDMS layer is necessary to achieve transfer.[5−10] Thick SWNT films are beneficial in applications ranging from solar cells to optical sensors, where device efficiency is correlated to the ability of the device to absorb all of the incident radiation. In addition, this process leaves the thin catalyst layer responsible for SWNT array growth behind on the growth substrate. Evidence of this, besides spectroscopic investigation, is that multiple regrowths can be achieved following transfer, similar to that described in recent work.[38] This means that the nanotubes remain free of metal, and these structures can therefore be manufactured with standard protocols, such as CMOS processing, where Fe is a premier contaminant. Since our first observation of this transfer process,[33] other reports have emerged with similar techniques for transfer of individual aligned SWNT structures to host substrates,[39,40] emphasizing the flexibility and already widespread interest in this facile technique. In particular, Hart's group[40] demonstrates the transfer of such blade structures of aligned nanotubes to flexible surfaces that can provide an excellent route to achieving highly conductive interconnects for electronics devices.

Shown in Figure 2 is a collection of images depicting a variety of transferred films produced from the technique illustrated in Figure 1a. Figure 2a shows a film of lines having a length slightly longer than the pitch between lines (resulting in a small overlap between adjacent lines, as shown in SEM image inset in Figure 2a) transferred to a clean SiO_2 surface that has been functionalized with aminopropyltriethoxysilane (APTES). Post-transfer, the SWNT film is spin-coated with ethanol and found to dry in such a way that no capillary-induced effects alter the continuity of the film. Upon drying, we find that the thickness of the film changes considerably and the nanotubes in the film appear to become more bundled and coagulated. However, the APTES layer promotes strong adhesion of the SWNT to the transfer surface, alleviating excessive cracking in the film structure that is typical of capillary force effects of such low-density structures during dry-

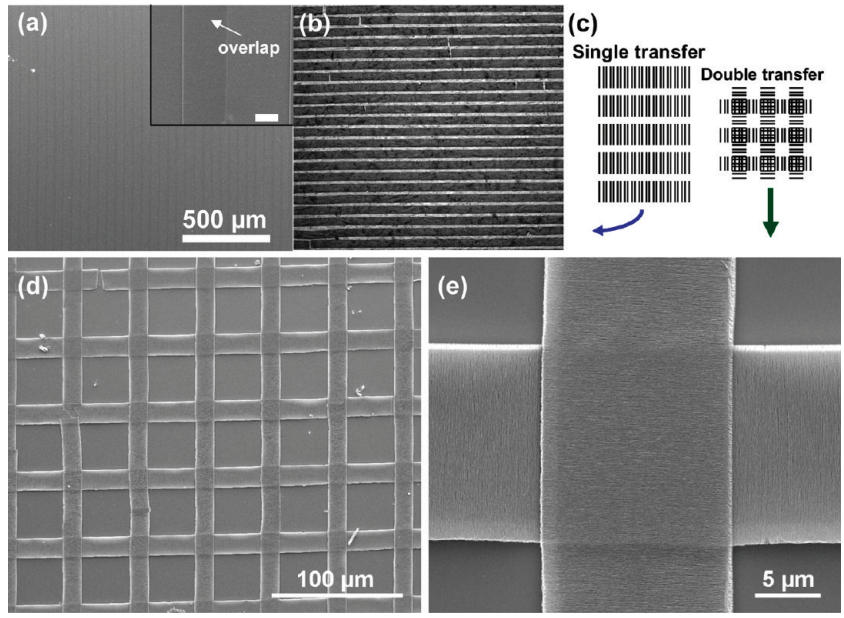

Figure 2. SEM images showing various films transferred *via* the technique shown in Figure 1. (a) Film transferred to APTES-functionalized SiO_2, with inset views showing the overlap region between lines. (b) Film transferred to a diamond window (corresponds to Figure 1c). (c) Scheme depicting the difference between an individual transfer and a dual transfer technique. (d) Zoomed-out SEM image of a grid pattern formed by two transfers, and (e) closer view of the grid pattern showing a single intersection of two individually transferred SWNT lines.

ing. Further images illustrating this concept are provided in the Supporting Information. This means that, utilizing an APTES adhesion layer, the transferred films can be subjected to wet processing for large-scale device fabrication. Figure 2b shows a film transferred to a diamond surface (corresponding to Figure 1c), where the length of the lines is smaller than the pitch between lines, resulting in an array of lines composed of aligned SWNTs. To depict how a single pattern can be made into a more complex design, Figure 2c shows the relation between a single transfer and a cross-bar (grid) pattern formed by two subsequent transfers of the same simple pattern, as shown in Figure 2d,e. Here, the second transfer is conducted with the stamp (growth substrate) rotated at an angle 90° relative to the initial pattern. The higher magnification SEM image in Figure 2e emphasizes the highly aligned nature of the SWNTs in a line intersection. The presence of a small crack in the transferred SWNT film shown in Figure 2d (upper left corner), as well as some cracks observable in Figure 2b, are typical "defects" in this process and arise from defects present during growth that cause gaps in the grown line structures. Since cracks only rarely occur along the many cleave planes that exist (due to the excellent SWNT alignment), these defects would only affect device or application performance if one fabricated the device such that charge transport occurred across this gap. Due to inefficient thermal and electrical transport normal to SWNT alignment, this means that device performance from such transferred structures is independent of these crack features. In addition, we find that the yield of transfer is very high—every attempt at transfer following the H_2O vapor etch resulted in complete transfer of the SWNT array film. We note that some transfers were not "perfect" (<20%) due to hand movement when removing the growth substrate or initially pressing the growth substrate to the host surface. This can be easily mitigated by the use of a mechanical apparatus to aid in completely reproducible transfer, even though we found transfer "by hand" to be efficient enough for the study presented here. Furthermore, although lower magnification SEM characterization (Figure 2) emphasizes the excellent alignment of the SWNT bundles in the arrays, the higher magnification image, shown in Figure 3, also emphasizes short segments of misaligned SWNTs among the well-aligned SWNT bundles. As will be discussed later, this is an important feature in properly characterizing anistropic properties of the SWNTs.

Overall, the ability to perform multiple transfers in a simple, dry approach raises the intriguing possibility of

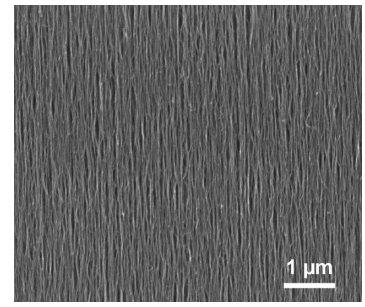

Figure 3. High-magnification SEM image of the alignment present in a general transferred SWNT structure, depicting both the good SWNT alignment as well as the misalignment in the film that is not obvious in lower magnification images.

complex micropatterning of metal-free aligned SWNT structures for a variety of applications. This can be useful in electronics and many other applications, where room-temperature transfer of metal-free aligned SWNTs can be integrated into devices that utilize the excellent anisotropic electrical and thermal properties of SWNTs. Moreover, this transfer process is not only limited to SWNTs, as similar contact transfer could be carried out on any material with similar structural characteristics. In any case, the ability to manipulate aligned SWNT structures to form patterns that are relevant for specific device applications is a concept we foresee to have a substantial impact on the future of carbon-nanotube-based applications. However, as a precursor to application development, it is first important to investigate simple, statistically sound techniques to characterize these aligned nanotubes, including the diameter distribution and the SWNT alignment. We now proceed by utilizing optical studies to characterize these features for aligned SWNT films transferred to IR windows.

Optical Properties of Transferred, Aligned SWNTs. The exciting optical properties of single-walled carbon nanotubes have led to the birth of a whole field of research devoted to understanding the physics of this unique one-dimensional family of molecules. As the rolling angle of the graphene sheet defines the electronic characteristics of SWNTs, investigation into the optical properties of metallic and semiconducting SWNTs has motivated the use of tools including absorption,[41] Raman spectroscopy,[42,43] and band gap fluorescence.[44,45] These optical techniques applied to material such as HiPco or CoMoCat SWNT have been performed routinely to gain straightforward insight into the SWNT makeup. However, as water-assisted CVD emerges as a key nanotube synthesis technique for a variety of applications, traditional and routine characterization methods no longer give the accurate information that one would like to achieve in such spectroscopic characterization. This requires spectroscopic analysis performed in the mid-IR wavelength range to accommodate the optical transitions shifted into this region. As this has yet to be demonstrated, it is questionable whether conventional visible and near-IR optical tools can be accurately utilized to assess the properties of these SWNTs. Unlike the optical response of small diameter SWNTs, such as HiPco, the response expected from the broad range of large diameter SWNTs in water-assisted CVD growth is a convolution of many individual features to result in broad first and second absorption bands spread throughout the near- to mid-IR range. In addition, specific (*n*,*m*) assignments can be ruled out due to the overlap of individual optical transitions to form broad absorption bands. Therefore, absorbance measurements in the IR yield promise for the characterization of general properties, such as the range of diameters present in the sample, which is typically the most sought feedback for synthesis techniques and for a general comparison between different as-synthesized materials utilized in applications. We note that the technique illustrated in Figure 1 is excellent for these studies because the films can be transferred to IR transparent windows (KBr) with no loss of nanotube alignment in the transferred film. Since it has been demonstrated that the absorption of radiation by SWNTs depends strongly on the polarization of the radiation relative to the SWNT alignment, fine control of the SWNT alignment direction relative to a fixed polarization of incoming radiation allows us to accurately assess the absorption features due to the nanotubes in the film.

Shown in Figure 4a,b is the angle dependence of the molar absorption coefficient for films transferred to KBr windows, calculated as $\varepsilon = A/cl_{\mathrm{eff}}$, where A is the absorbance at an angle θ, ($A(\theta = 90°)$ has been subtracted), c is the concentration (mol/cm^3), which is calculated from the known carbon density of $\sim$55 mg/cm^3, and l is the thickness of the SWNT film ($l_{\mathrm{eff}} = 0.54$ μm). Data with the raw value of ε (no subtraction) are shown in the Supporting Information. In order to characterize the angular dependence, measurements are taken at increments of 10° with respect to a fixed polarization of light utilizing a rotating sample holder which can be heated and held under vacuum (7×10^{-7} Torr). Data taken when the radiation field is normal to the SWNT alignment (90°) are then subtracted from all other spectra (in addition to the uniform background from KBr) to indicate the polarization dependence of only optically allowed SWNT-related features.

Shown in Figure 4b is a contour plot of the angular-dependent data, with the three emergent polarization-dependent absorption features further labeled in a plot of the linear dichroism (LD) (Figure 4c) that we interpret as the (i) long-wavelength absorption peak extending into the terahertz frequency range that represents absorption partially due to free carriers ($<$1000 cm^{-1}), and (ii,iii) first ($\sim$2600 cm^{-1}) and second ($\sim$5300 cm^{-1}) excitonic interband transitions for semiconducting SWNTs (E_{11}^{SC} and E_{22}^{SC}, respectively). The origin of the long-wavelength peak is still not fully understood.[46−49] Measurements in the far-IR consistently show that enhancing the free carrier population (*i.e.*, by doping the SWNTs) increases the intensity of this peak,[48] but other reports suggest influence of interband transitions from the narrow-gap semiconducting (SC) SWNT population.[47,48] Recent experiments performed on our films show little apparent temperature dependence of the line shape and magnitude of this far-IR absorption, except with a strongly negative complex and real dielectric constant emphasizing a strong metallic contribution to this peak.[50] Therefore, this peak will be loosely referred to as the "free carrier absorption" based on its apparent indication of metallicity in our experiments. However, it is important to note that this is not simply a Drude-like absorption and is still not fully established

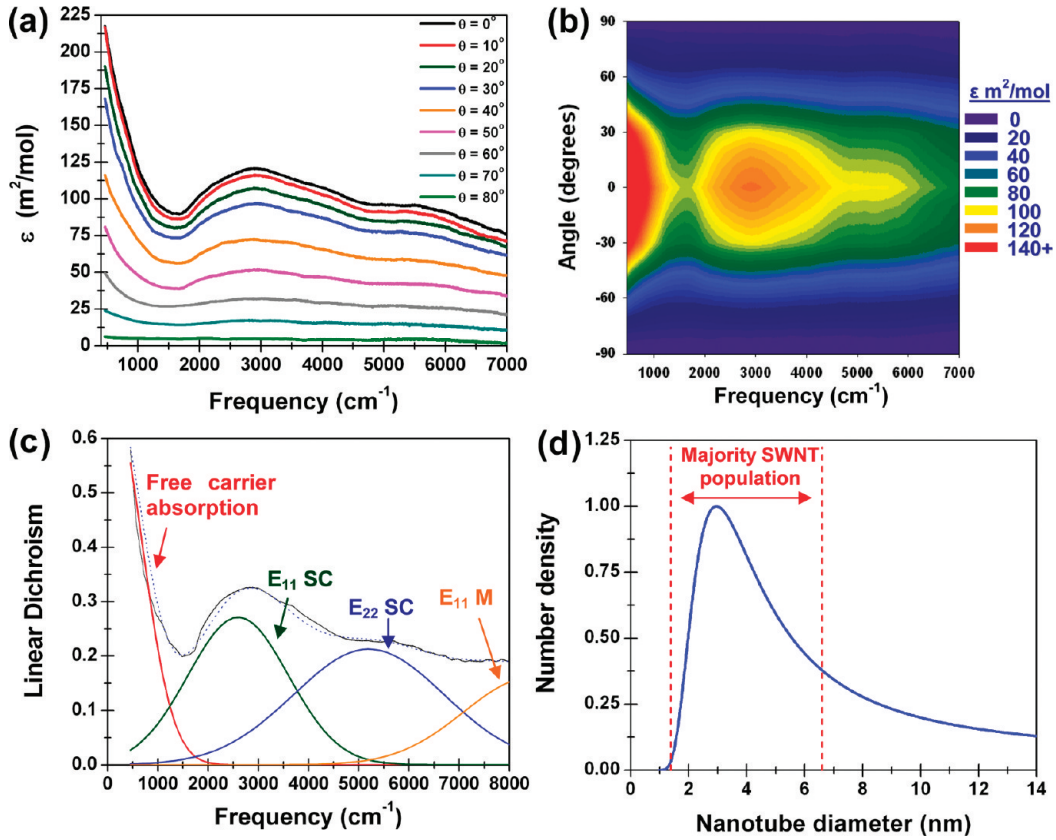

Figure 4. (a,b) Angular dependence of the frequency-dependent molar absorption coefficient, ε, for aligned films transferred to KBr windows, taken in increments of 10°, with ε(θ = 90°) subtracted to represent the absorbance due only to the aligned nanotubes. (b) Contour graph of this, emphasizing the emergence of interband SWNT transitions and the free carrier absorption. (c) Fitting scheme to the linear dichroism (θ = 0° data shown in (a)) depicting relative contributions from the semiconductor optical transitions (E_{11}^{SC}, E_{22}^{SC}) and the free carrier absorption. (d) SWNT diameter distribution extrapolated from fit in (c) and utilizing eq 2.

in origin. On the other hand, the interband (excitonic) transition features for the SWNTs in the array are well-established and represent absorption due to carriers being excited across the energy gap of the first and second pairs of van Hove singularities in the SWNT electronic density of states.[51]

For an individual SWNT, excitonic transitions in 1-D confined structures lead to electronic transitions having narrow (Lorentzian) line shapes. However, one can interpret the broad optical transition features associated with the aligned samples shown in Figure 4c as a collection of a large ensemble of overlapping Lorentzian curves which can be equally represented by a Gaussian line shape. We therefore utilize a fitting technique where each of the interband transition features (E_{11}^{SC}, E_{22}^{SC}, and E_{11}^{M}) is fit with a broad Gaussian line shape. To account for the presence of the free carrier absorption band, we also utilize a Gaussian fit centered at ~95 cm^{-1}, which is the general vicinity of the broad terahertz absorption peak.[46−49] Although the detailed line shape of this peak is not expected to be best represented with a Gaussian fit, a sharp cutoff near 400−450 cm^{-1} due to the light source and beamsplitter combination makes it impossible to resolve any line shape from this peak. Therefore, we apply a Gaussian fit as a first-order result to account for the presence of this peak without further information of shape that would come from lower frequency measurements.

As shown by the dotted line in Figure 4c, the fitting process yields a reasonable fit to the normalized absorption data. The distinct signature of the E_{11}^{SC} optical transitions in Figure 4c makes it possible to infer information about the diameter range of the SWNT population (Figure 4d). In order to quantitatively analyze this absorption envelope to determine SWNT diameter information, a relation between the optical transition energy, the band gap, and the diameter must be established. We can therefore express the measured E_{11} transition energy (E_{opt}) as a linear combination of the band gap energy (E_g), the exciton binding energy (E_b), and the self-energy (E_s), as

$$E_{opt} = E_g - E_b + E_s \quad (1)$$

which are each illustrated by the scheme inset in Figure 5. Constructing the form E_{opt} from components E_g, E_b, and E_s as described elsewhere,[52−57] we can rewrite eq 1 as

$$E_{opt} = \frac{2\gamma_0 a_{C-C}}{d} - \frac{\varepsilon^{-\alpha}}{d} + 0.55\frac{2p}{3d}\ln\left[\frac{9d}{2p}\right] \quad (2)$$

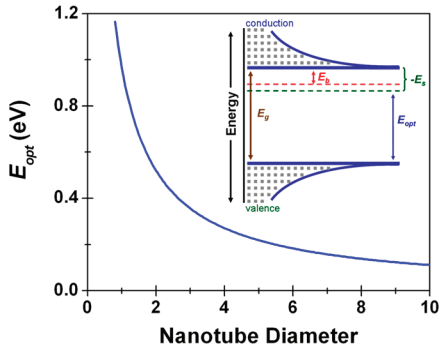

Figure 5. Optical transition energy plotted as a function of the nanotube diameter, according to eq 2 and the parameters discussed in the text. Inset is a scheme depicting the E_{11} optical transition for a carbon nanotube, with each energy value labeled in accordance with eq 1.

where d is the nanotube diameter, a_{C-C} is the interatomic carbon−carbon distance (0.142 nm), θ_0 is a constant from tight-binding calculations, ε is a parameter describing the effective dielectric constant, α is a scaling parameter for ε, and p is an integer describing the order of the transition. It should be noted that additional many-body terms could be included to give (n,m) specificity to the optical transition energies.[58−60] However, these are higher order corrections that lose meaning with the broad diameter distribution present in our samples and are therefore neglected. Therefore, the ability to achieve a reliable diameter distribution from the range of measured transition energies is inherently dependent on the accuracy of the parameters in eq 2. In all cases here, the measurements were performed in vacuum, allowing us to fix $\varepsilon = 1.842$[59] and the adjustable parameter α to 1.4 as described by Perebeinos *et al.*[53] For the band gap energy, the parameter γ_0 was fixed at 2.5 eV, which was chosen due to (i) excellent correspondence between the relation in eq 2 and the experimentally determined optical transition energies for smaller diameter SWNTs (Supporting Information),[61] and (ii) experimental determination of this value through STM measurements by Odom *et al.*[52] The parameter p was fixed at 1 because we are analyzing the E_{11}^{SC} optical transition. Therefore, we expect eq 2 and these parameters to best capture the physics associated with optical absorption and therefore be the most accurate, both physically and quantitatively, in assigning optical transition energies.

In order to assess the validity in using eq 2 to describe optical transition energies, we plot the optical transition energy as a function of diameter with these parameters, as shown in Figure 5. Most importantly, this relation yields optical transition energies agreeing well with measured values from the experimental Kataura plot.[61] The difference in E_{11}^{SC} transition energies in mod1 and mod2 SC SWNTs is not captured in eq 2 and is expected to diminish as the SWNT diameter becomes larger (it could be captured by extending the exciton binding energy term in eq 2 beyond the leading term[58,59]). Overall, the accuracy of eq 2 in describing optical transition energies is most dependent on limited experimental data for the extrapolation of exciton binding energies and self-energies into the range of large diameter SWNTs. Until now, most experiments have been performed in aqueous environments, where spectroscopy is limited to the near-IR and high-frequency edge of the mid-IR range due to the overlap of water absorption. Therefore, we expect this simple model to be the most accurate from the current state of experimental investigation into these effects, even though a better treatment of many-body effects in individualized, larger diameter SWNTs in well-controlled environments is still necessary.

In order to extract a diameter distribution, eq 2 is solved for d (as a function of E_{opt}), and the measured envelope of E_{11}^{SC} transition energies is mapped onto the diameter distribution. To analytically solve eq 2, the ln(9d/2p) term is expanded into a series, and only the first leading term of the series is utilized in the calculation to obtain the distribution shown in Figure 4d. We also observe that the leading $1/d$ dependence of the Coulomb self-energy term can alternatively be taken into account by scaling the value of γ_0 to ~4.6 eV (scaled to give a similar E_{opt} compared to that when E_s is explicitly considered) and disregarding the part of eq 2 describing the self-energy. This slightly decreases the width of the distribution but still describes the majority SWNT diameter population accurately. This represents a route to reduce the difficulty of solving eq 2 (with the logarithmic relation from E_s) but still gives empirically correct transition energies.

Upon inspection of the distribution shown in Figure 4d, it is evident that the Gaussian fit applied to the envelope of E_{11}^{SC} transitions is only accurate to first-order and likely misrepresents the shape of the real envelope at the extrema (large and small diameter edges). This is most apparent by a long tail extending to large diameters and a nonzero probability of SWNT having $d = \infty$. Nonetheless, one can determine from this fit the majority SWNT diameter range, which is the important information sought through this technique. From Figure 4d, the diameter range appears peaked at ~2.7 nm with a large population of nanotubes having diameters greater than 3 nm, which is consistent with TEM characterization of SWNT material grown *via* this technique,[29−31] as well as observations of SWNTs present in the typical water-assisted supergrowth process of Hata and co-workers.[15,22] As a result, this process of utilizing polarization-dependent IR absorption in highly aligned SWNT samples is a promising route toward establishing the diameter distribution of a sample having SWNTs in a diameter range consistent with the water-assisted CVD technique.

Recently, we have shown that the electrical properties of SWNT films made utilizing the technique shown in Figure 1 can be altered by air exposure of the film and

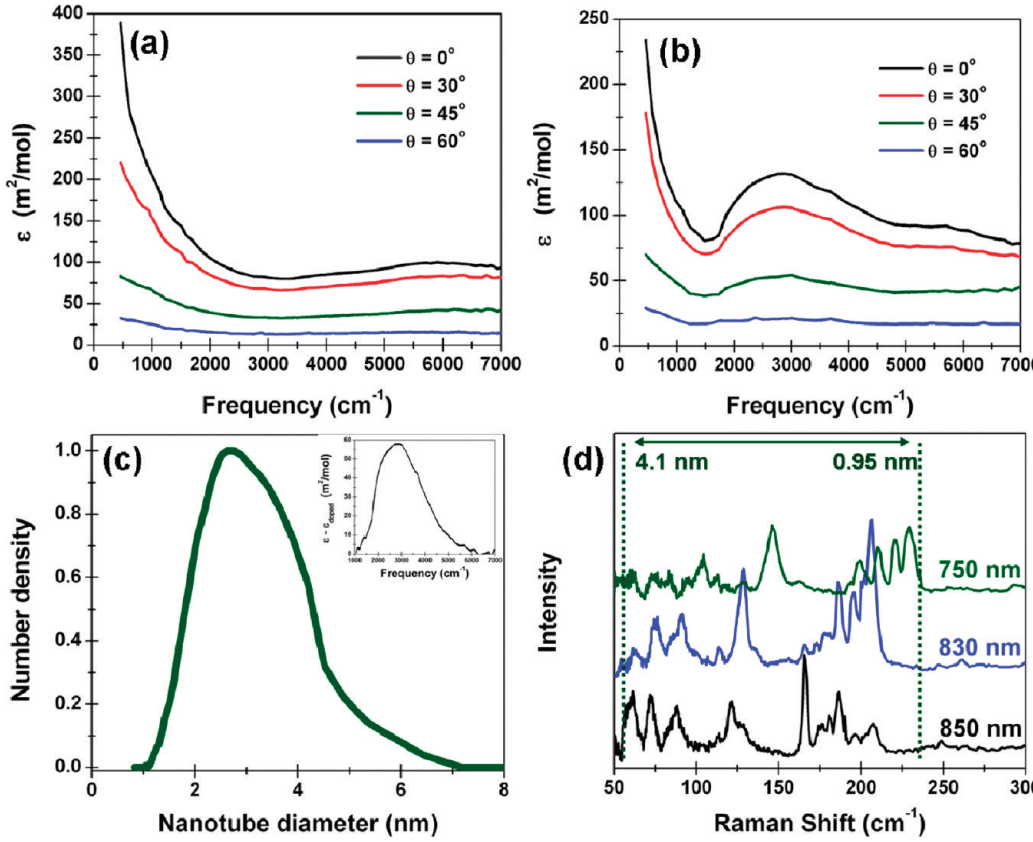

Figure 6. Angular dependence of the IR molar absorption coefficient for a SWNT film (a) following a long (~4 month) air exposure, and (b) the same film in (a) after a 5 min anneal at 100 °C. (c) Diameter distribution obtained by utilizing eq 2 with the quenched E_{11}^{SC} contribution evident from subtraction of θ = 0° spectra in (a) and (b). Inset in (c) is the IR molar absorptivity subtraction, from which the diameter distribution was extracted. (d) Radial breathing modes (RBM) in resonant Raman spectroscopy taken with 750, 830, and 850 nm excitations. The dotted lines mark the general range of diameters (calculated *via* $\theta_{RBM} = 227/d$, from ref 55) observed in this technique, which are also labeled.

subsequent vacuum annealing.[62] Interestingly, with over a week of exposure to air, vacuum annealing of the SWNT films resulted in absolutely no change in the observed optical properties. However, after leaving the films in the laboratory for ~4 months exposed to air, a distinct change in the optical absorption spectra was observed, as shown in Figure 6a. The same anisotropic optical absorption as shown in Figure 4 is observed in this case, except that the peak describing the envelope of E_{11}^{SC} optical transitions is no longer distinguished in the spectra. After taking the data in Figure 6a, we subjected the film to 5 min of vacuum annealing (100 °C, 7 × 10^{-7} Torr), after which the optical absorption spectrum of the pristine SWNT film was restored, as shown in Figure 6b. Therefore, some constituent of air in low abundance resulted in a p- or n-type doping effect on the SWNTs, shifting the Fermi level of the nanotubes into the valence (conduction) band, respectively, and bleaching the E_{11}^{SC} optical transitions. The specific constituent is unknown: experiments designed to test this by utilizing purely O_2, CO_2, or H_2O exposed to the SWNT film for up to 30 min in the vacuum cell resulted in no observable effect in the optical spectra of doping due to physisorption, even though O_2 has been reported in the past to facilitate charge transfer in solution to bleach optical transitions in small diameter SWNTs.[63] This general phenomenon has also been reported through acid-doping (p-doping) in the past[64−66] and therefore appears to be a reasonable explanation. In addition, consistent with a shift of the Fermi level to a position between the first and second mirror van Hove singularities in the density of states, the envelope of E_{22}^{SC} optical transitions is generally unaffected. Comparison of Figure 6a,b emphasizes a difference not only in the E_{11}^{SC} optical transitions but also in the long-wavelength free-carrier absorption. The enhancement of the magnitude of this free-carrier band is an additional indication of an enhanced free-carrier population, as one would expect if the change in the spectra was due to doping. After vacuum annealing, the free-carrier absorption returns to a level identical to that for the previously measured pristine SWNT film in concert with the return of the envelope of E_{11}^{SC} optical transitions. The behavior of the free-carrier absorption is similar to that observed by Itkis *et al.* upon doping of HiPco films.[46]

The sensitivity of the E_{11}^{SC} optical transitions chemical doping presents an alternative route to analysis of the diameter distribution through a comparison of the doped *versus* pristine SWNT film. In order to do this, we took the difference between the normalized (differ-

ence between 0 and 90° absorption, as shown in Figure 6a,b) IR spectra for the doped and pristine films. In order to account for the enhanced free-carrier band in the doped SWNT film, a Gaussian fit was applied similarly to that in Figure 4c, except with a varying amplitude. This ensures that the result of the subtraction of the two spectra was not influenced by the enhanced free-carrier absorption and therefore is representative of the characteristic shape of the E_{11}^{SC} absorption envelope. Again, utilizing eq 2 to relate the envelope of E_{11}^{SC} transitions to the diameter distribution yields a distribution with nearly the same shape and peak position as shown in Figure 4c, except with a more realistic large diameter tail. The use of subtracted optical absorption in SWNT films where the E_{11}^{SC} is bleached (doped) *versus* when the E_{11}^{SC} is strongest (pristine) gives the most accurate information about the shape of the E_{11}^{SC} absorption band and therefore is expected to give the most accurate fit of the diameter distribution. This provides a route where special sample preparation is not necessary to obtain a diameter distribution, as this can be performed just as easily on misaligned films using the formalism presented in eq 2.

Further analysis of the diameter distribution from radial breathing modes in resonant Raman spectroscopy, as shown in Figure 6d, also emphasizes a broad diameter distribution that has species ranging from below 1 nm in diameter up to ~4 nm based on the relation, $\theta_{RBM} = 227/d$.[67] The caveat to this measurement technique is that the signature of the majority of SWNT species is in the form of higher order transitions ($E_{22}-E_{55}$ for SC SWNT), which makes a quantitatively accurate diameter distribution challenging to obtain. Nonetheless, resonant Raman spectroscopy is a useful tool for the identification of the presence of these SWNT species and can be utilized as a technique complementary to IR absorption measurements. However, IR absorption that can be performed in an FTIR system (readily available in nearly every laboratory) can be distinguished as a technique that can quickly and effectively be utilized to give an estimate of the majority SWNT diameter distribution for such larger diameter SWNT species in accordance with Figures 4d and c.

In order to verify the diameter distributions obtained *via* IR absorption, we performed AFM analysis of surfactant-suspended SWNTs from carpets as an alternative technique to estimate the general range of diameters in the sample. To suspend the SWNTs, the nanotubes were detached from the catalyst layer and tip-sonicated in a sodium deoxycholate/water solution for 2 h with an approximate concentration of 100 mg/L. Following this, a decant was prepared by ultracentrifugation at 200 000*g* for 2 h. The resulting solution was diluted and spin-coated onto a clean mica surface for AFM imaging. A typical AFM scan of the nanotubes characterized, as well as a distribution of ~120 manually assigned nanotube heights, is shown in Figure 7. It should be noted that the tip sonication period resulted in substantial cutting of the nanotubes, leaving them in pieces near 1 μm long, on average. Diameter analysis was performed to characterize the nanotubes identified as individuals by forming height profiles along the nanotubes and monitoring whether there was any indication of bundling in the measured tubes (which is often evident in broken bundles by intersections of tubes into a bundle). In general, the distributions measured appear to correlate well to the majority diameter distribution characterized *via* IR spectroscopy and eq 2, and provides a similar picture to distributions made from TEM images[32] and average catalyst particle sizes reported through plan-view TEM[28] utilizing the same water-assisted CVD process. As noted previously, the fits from the IR spectra are slightly more inaccurate at the extrema of the distribution, especially in the case of the fit from Figure 4d, where the long tail inaccurately represents the large diameter population. The fit from Figure 6c best represents the larger diameter SWNT species, but both distributions underestimate the small diameter SWNTs present. Data from Raman spectroscopy (750 nm excitation, Figure 6d) indicate a clear presence of these smaller diameter SWNTs through the E_{22}^{SC} optical transition. The inability of this technique to accurately capture those species is likely due to the very long and broad tail of the E_{11}^{SC} envelope that extends into the near-IR and overlaps with the higher order transitions from the majority SWNT species. However, the key point here is that these fits generally capture the majority SWNT population in a statistically sound approach and therefore represent a powerful tool for diameter analysis for an unknown CNT sample without the requirement of specialized sample preparation.

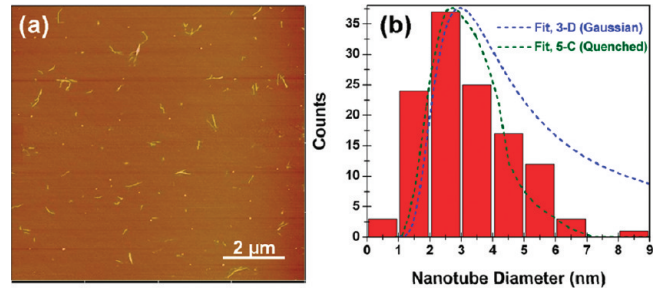

Figure 7. (a) Representative AFM image obtained following dispersion and spin coating of a CVD-grown SWNT onto clean mica surfaces, and (b) diameter distribution of 122 individual nanotubes taken *via* AFM. Overlaid on the distribution is the calculated diameter distribution using IR data and eq 2 as shown in Figure 3d (blue) and Figure 5c (green), emphasizing good general agreement between the majority SWNT population determined from IR absorption measurements.

Characterization of Alignment for Long, Aligned SWNTs. In addition to the SWNT diameter distribution, another key feature that is useful to analyze is the alignment present in the SWNT film. Alignment is also a quantity of interest since it is a primary aspect of determining the elec-

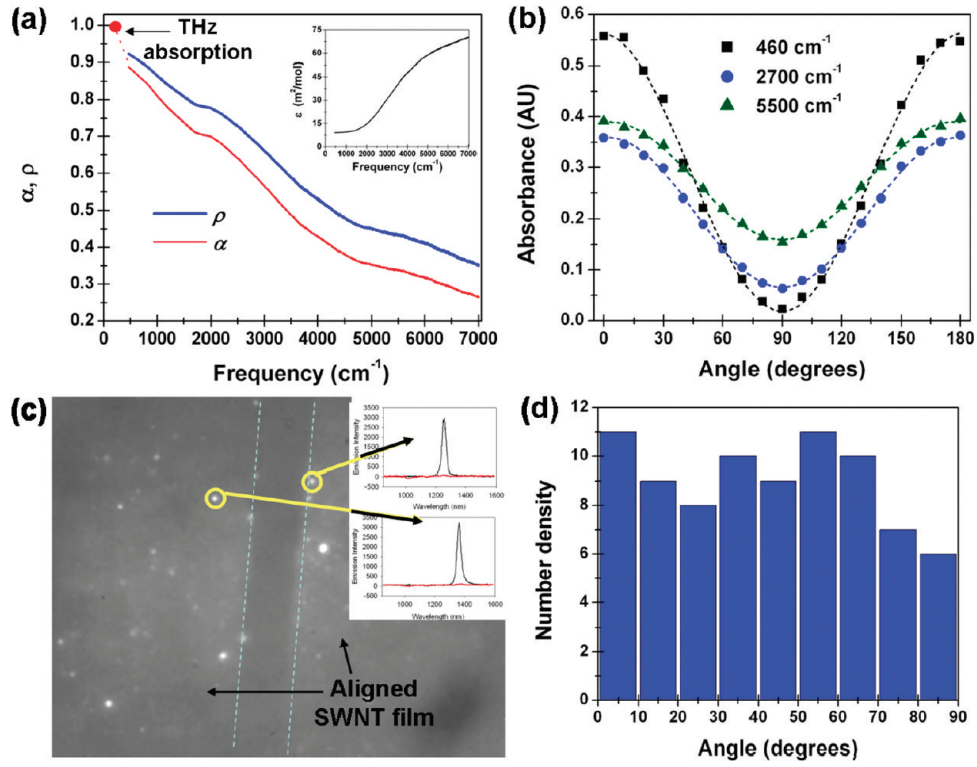

Figure 8. (a) Polarization and optical absorption anisotropy calculated in accordance with eq 3. The red point and dotted line is an extrapolated fit to data taken in the THz as described in ref 21. Inset is a plot of the smooth background of ε obtained in θ = 90° spectra. (b) Angular dependence of the absolute absorbance for the three distinct peaks labeled in Figure 3c. Dotted lines represent best fits achieved with a generalized $\sin^2(\theta)$ + C function. (c) Near-IR image of fluorescence emission from a dry, transferred aligned SWNT film to a glass coverslip. Inset shows representative emission spectra to emphasize that each bright spot corresponds to individual SWNT emission sites. Similar to transferred films shown in Figure 2b, there is a gap between the SWNT in the aligned film where no emission spots are observed. (d) Angular dependence of a collection of 81 total nanotubes measured by tracking the polarization dependent emission intensity as a function of angle (in 10° increments).

trical, thermal, and mechanical properties of structures composed of SWNTs. The anisotropic electrical and thermal transport properties of SWNTs in films make a proper measurement of alignment crucial in understanding transport mechanisms observed or expected from a SWNT material. The strongly anisotropic absorption of polarized radiation by SWNTs has made polarized spectroscopic techniques, including polarized Raman spectroscopy[68−70] and/or polarized absorption spectroscopy,[71−73] useful techniques for alignment characterization. Utilizing well-aligned SWNT samples made by the process illustrated in Figure 1, we can investigate the alignment in the film and determine the degree of alignment as a function of wavelength. Shown in Figure 8a is a plot of the optical absorption anisotropy, α, and the polarization, θ, as a function of the parallel absorption ($\Lambda_\parallel$) and perpendicular absorption ($\Lambda_\perp$) as defined:[69]

$$\alpha = \frac{\Lambda_\parallel - \Lambda_\perp}{\Lambda_\parallel + 2\Lambda_\perp}, \rho = \frac{\Lambda_\parallel - \Lambda_\perp}{\Lambda_\parallel + \Lambda_\perp} \quad (3)$$

Here, α is a quantity that can be compared to the nematic order parameter, which was calculated to be 1 for similar films in recent THz (~2 THz) absorption experiments,[21] as noted in Figure 8a. It should be noted that the radiation length scale is not proportional to wavenumbers, which makes the THz point in Figure 8a appear higher than the data presented at greater frequencies. However, on a plot where the parameters are plotted as a function of θ, this is not the case. The inset in Figure 8a is the $\Lambda_\perp$ background, which appears to be greatest in the vicinity of the interband optical transition features or generally in the higher energy region of the spectra.

Interestingly, the magnitudes of both α and θ appear to be strongly dependent on the wavelength at which these quantities are calculated. At the lowest energies available to these experiments, it is clear that the values of the quantities in eq 3 approach 1, consistent with polarization-dependent measurements at ~2 THz. However, on the high energy side of the spectra, the anisotropy appears to be lower and the values of α and θ drop to between 0.3 and 0.45, where the greatest "background" absorption takes place. This change in the anisotropic absorption characteristic of the film as a function of wavelength is also illustrated in Figure 8b, which shows the angle-dependent raw absorption data (not normalized) for three specific points in the (i) free-carrier absorption region (460 cm^{-1}), (ii) peak of the envelope of E_{11}^{SC} optical transitions (2700 cm^{-1}), and

(iii) peak of the envelope of E_{22}^{SC} optical transitions (5500 cm^{-1}). In each case, the data points taken in increments of 10° give an excellent fit to a generalized $\sin^2(\theta) + C$ function (the dotted line in Figure 8b), which is typically observed for aligned SWNT structures in polarized absorption measurements. Most evident from these data is that the free-carrier absorption is the strongest anisotropic feature, followed by the E_{11}^{SC} transitions and then the E_{22}^{SC} transitions. This raises an interesting question regarding the mechanism behind the different absorption anisotropy in each of the SWNT IR absorption features. In the first case, this could be influenced from cross-polarized optical transitions.[74−76] Recent studies have shown that bundled SWNTs (which are the majority of the SWNT array species) can exhibit a depolarization effect[74] that can change the selection rules for absorption of light with a field direction normal to the SWNT long axis. This means that bundled SWNT can exhibit forbidden $E_{n,m}$ optical transitions instead of only the allowed $E_{n,n}$ transitions, which are always the dominant polarized transitions in individual SWNT experiments. Subtraction of expected E_{11}^{SC} and E_{22}^{SC} absorption bands from the raw data does not indicate any apparent changing baseline for the polarization-dependent IR spectra compared to that observed with $\theta = 90°$. As a result, we believe that any effect from the optically forbidden transitions to be broad (and hence weak) and generally featureless—making it impossible to trace in these measurements. Therefore, we focus on another important consideration in the anisotropy of the film, which is the effect of misalignment and a wavelength-dependent length scale that is probed in absorption measurements. This is emphasized by the optical absorption anisotropy that is strongly dependent on wavelength, as shown in Figure 8a. One explanation for the changing anisotropy is a threshold length scale for misalignment to occur in the film. Although zoomed-out SEM images always indicate what appear to be extremely well-aligned bundles of SWNT, closer views typically reveal that many of the nanotubes stray and remain misaligned over length scales of a few hundred nanometers, whereas the bundles (which are typically most evident in SEM) remain rigid and well-aligned as depicted in Figure 3. Neutron scattering experiments performed on aligned CNT arrays indicate the presence of well-aligned CNTs among a population of misaligned CNTs.[77] Other recent analysis has emphasized that many SWNTs grown in both alcohol-assisted and water-assisted CVD processes tend to exist, at least partially, as individuals or small bundles.[78] With this in mind, we characterized alignment utilizing photoluminescence from a dry, aligned SWNT film transferred to a glass coverslip, as shown in Figure 8c. As shown, many bright (and dimmer) spots are observed corresponding to emission sites from small diameter SWNTs present on the surface of the sample and within the sample, respectively. When the emission spectra from individual spots (inset in Figure 8c) were analyzed, the narrow line shape and single emission peaks along with the individual SWNT polarization dependence emphasize these spots likely correspond to individual semiconducting SWNTs. However, tracking the polarization dependence of a total of 81 individual bright emission spots, we observed that the SWNTs appear to have no apparent orientation, as shown in Figure 8d, contrary to other measurements. This measurement illustrates the substructure of the nanotube array that consists of individual SWNT or small bundles straying from the overall alignment direction. As a result, this substructure of the array could play a role in affecting the anisotropy of the film in IR absorbance measurements. The presence of dim and bright emission sites within the SWNT lines indicates this is from SWNTs located throughout the SWNT line, and the lack of anisotropy is a combination of a short length scale excitation probe (785 nm) and a substructure of individual SWNT and small bundles amidst a well-aligned primary structure of highly bundled SWNTs. If the region of misalignment in a nanotube is much greater than the localization length of a bound exciton, off-axis absorption should be expected to scale with the length of the misaligned SWNT.[79] Furthermore, with a fixed average length scale on which misalignment occurs, increasing the wavelength of incident radiation should also damp the absorption from the misaligned population. Therefore, the wavelength-dependent background could be strongly influenced by misalignment inherent to the structure of vertically aligned SWNT grown *via* the water-assisted CVD process.

A complementary measure of alignment can be performed *via* G-band polarized Raman spectroscopy, as shown in Figure 9. The Raman data are well-fit to a generalized fourth-power sinusoidal relation ($C + \sin^4(\theta)$), in agreement with previous measurements[80] and the general form for the angular scattering intensity of electromagnetic radiation for a collection of polarizable cylinders. The ratio of $G_{parallel}/G_{perp}$ in this case is ~3.5, which is generally consistent with the absorption anisotropy at wavelengths approaching the near-IR. Although this represents a reasonably well-aligned structure, it is a value much lower than that observed in recent conductivity measurements for similar films, with anisotropy (conduction parallel/perpendicular to alignment) greater than 100 at room temperature. Previous studies have established that, for HiPco SWNT (length <1 μm),[81] the anisotropy in conduction is similar to the G-band ratio in polarized Raman spectroscopy. However, when the SWNT length is much greater than the excitation wavelength, the anisotropy measured is not representative of anisotropy that would arise in the physical performance of the film in an application but perhaps indicative of the substructure of the aligned SWNT film that is less important. Not only does this emphasize the usefulness of long SWNTs for applications

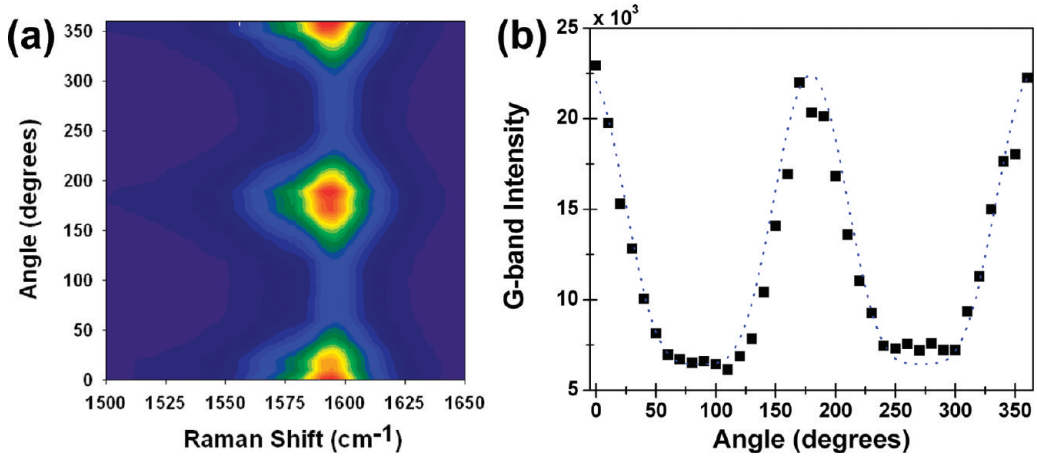

Figure 9. Polarized Raman spectra with 785 nm excitation showing G-band as a function of angle both as (a) a contour map and (b) a plot showing maximum G-band intensity as a function of angle, with the dotted line depicting a generalized $\sin^4(\theta) + C$ fit. Raman response is measured with scattered light in parallel polarization to incident light while sample is rotated.

where alignment may be necessary to yield device performance, but it also emphasizes the need for a better range of "tools" to accurately characterize the long, larger diameter SWNT species typically produced in the CVD process. It seems reasonable that the measure of alignment for long SWNT films through optical techniques should be conducted on a length scale that is comparable to the length of the SWNT. This means that optical excitation in the visible and near-IR does not yield equivalent information about the film alignment for the long SWNT as it may for HiPco or other submicrometer length SWNTs that have lengths comparable to that of the incident excitation. From the work presented here, we believe that IR absorbance can be distinguished as an effective tool for the characterization of the alignment in this way, in addition to analysis of the diameter range of the SWNT population. In addition, we foresee the adaptation of other common resonant optical characterization techniques into the IR to properly assess the large diameter SWNT population that is commonly produced in the CVD technique but remains relatively unstudied through existing optical techniques. As nanotubes grown in the CVD process continue to appeal to applications, it is of great importance to have equivalent tools to study and compare the optical properties of these nanotubes compared to those tools which have been developed in the past decade for their smaller diameter counterparts.

CONCLUSION

We demonstrate here a technique for dry transfer of horizontally aligned structures of well-aligned carbon nanotubes applicable to wafer-scale processing technology, with the ability to tailor patterns utilizing multiple transfers for advanced device design. Utilizing these films transferred to optical windows, we perform in-depth analysis of polarized infrared absorbance, extracting approximate diameter distributions and providing insight on alignment and anisotropy characterization in the film. We demonstrate this to be a technique useful for the case of polarized incident radiation and aligned SWNT samples, as well as unpolarized incident radiation and misaligned (doped) SWNT samples, in obtaining an accurate distribution of the SWNT diameters. Finally, utilizing near-IR polarized photoluminescence and Raman spectroscopy, we emphasize key features that may influence the anisotropy—such as misalignment occurring over length scales much smaller than the total SWNT length. This work provides insight into characterization and scalable processing of a class of CVD-grown CNT materials that are emerging as key components in many current applications.

EXPERIMENTAL DETAILS

Vertically aligned SWNT arrays were synthesized through CVD utilizing water-assisted growth and either hot filament[27] (atomic hydrogen) or hydrazine[28] reduction for catalyst activation. In order to grow SWNT arrays, a mixture of C_2H_2, H_2, and H_2O was introduced under vacuum (1.4 Torr) to a growth substrate heated to 750 °C. Details of the growth procedure and parametric information of nanotubes obtained are extensively discussed elsewhere.[29−32] In order to pattern the growth substrates, optical lithography was utilized to create catalyst pads between 0.5 and 2 μm wide and spaced by 50 μm across a 4 in. p-doped Si wafer having a 0.5 nm thick Fe catalyst layer. Films were formed by detachment of the aligned SWNT from the catalyst *via* H_2O vapor etching[33] in the CVD system for 3−5 min, and SWNT transfer was achieved by contact transfer as illustrated and discussed in Figure 1.

In order to carry out optical absorption experiments, aligned SWNT films are transferred to a clean, polished KBr window which is positioned in a vacuum cell with the film exposed to vacuum and another KBr window on the opposite side. Absorption spectra are taken with a KBr beamsplitter and either a white or IR light source and a DTGS detector in a Thermo Nicolet Nexus 870 FTIR system. Polarized fluorescence is measured on a custom-built near-IR microscope system discussed previously,[34]

where polarization-dependent data are taken by changing the polarization of the incoming laser excitation with respect to the alignment in the sample. The combination of a 785 nm laser and a near-IR detector (900−1700 nm) limits the observation of only small diameter SWNTs ($d < 1.5$ nm).[63] Polarized Raman data are taken utilizing a 785 nm diode laser with a rotating sample mount, whereas additional Raman data taken at multiple laser lines were obtained using a tunable Ti:sapphire laser, similar to that in ref 22.

Acknowledgment. The authors thank R.B. Weisman for use of the NIR microscope for fluorescence measurements, and C.L.P. thanks F. Leonard, S. Sinton, C. Cates, and others from Lockheed Martin for enlightening discussions, and S. Ripley for valuable experimental assistance. This work was supported by the Lockheed Martin LANCER program at Rice University.

Supporting Information Available: Illustration of experimental technique utilized for polarized absorption measurements inside the FTIR system, raw angle dependent molar absorption coefficient plotted as a function of frequency, and comparison of model in eq 2 to experimentally measured optical transition energies for smaller diameter SWNTs. This material is available free of charge *via* the Internet at http://pubs.acs.org.

REFERENCES AND NOTES

1. Chang, J. C.; Brewer, G. J.; Wheeler, B. C. A Modified Microstamping Technique Enhances Polylysine Transfer and Neuronal Cell Patterning. *Biomaterials* **2003**, *24*, 2863–2870.
2. Sun, Y.; Rogers, J. A. Fabricating Semiconductor Nano/Microwires and Transfer Printing Ordered Arrays of Them onto Plastic Substrates. *Nano Lett.* **2004**, *4*, 1953–1959.
3. Menard, E.; Nuzzo, R. G.; Rogers, J. A. Bendable Single Crystal Thin Film Transistors Formed by Printing on Plastic Substrates. *Appl. Phys. Lett.* **2005**, *86*, 093507.
4. Meitl, M. A.; Zhou, Y.; Gaur, A.; Jeon, S.; Usrey, M. L.; Strano, M. S.; Rogers, J. A. Solution Casting and Transfer Printing Single-Walled Carbon Nanotube Films. *Nano Lett.* **2004**, *4*, 1643–1647.
5. Zhou, Y.; Hu, L.; Gruner, G. A Method of Printing Carbon Nanotube Thin Films. *Appl. Phys. Lett.* **2006**, *88*, 123109.
6. Zhu, Y.; Lim, X.; Sim, M. C.; Lim, C. T.; Sow, C. H. Versatile Transfer of Aligned Carbon Nanotubes with Polydimethylsiloxane as the Intermediate. *Nanotechnology* **2008**, *19*, 325304.
7. Hur, S.-H.; Khang, D.-Y.; Kocobas, C.; Rogers, J. A. Nanotransfer Printing by Use of Noncovalent Surface Forces: Applications to Thin Film Transistors That Use Single-Walled Carbon Nanotube Networks and Semiconducting Polymers. *Appl. Phys. Lett.* **2004**, *85*, 5730.
8. Kumar, A.; Pushparaj, V.; Kar, S.; Nalamasu, O.; Ajayan, P. M.; Baskaran, R. Contact Transfer of Aligned Carbon Nanotube Arrays onto Conducting Substrates. *Appl. Phys. Lett.* **2006**, *89*, 163120.
9. Wang, T; Carlberg, B; Jonsson, M.; Jeong, G.-H.; Campbell, E. H.; Liu, J. Low Temperature Transfer and Formation of Carbon Nanotube Arrays by Imprinted Conductive Adhesive. *Appl. Phys. Lett.* **2007**, *91*, 093123.
10. Kang, S. J.; Kocobas, C.; Kim, H.-S.; Cao, Q.; Meitl, M. A.; Khang, D.-Y.; Rogers, J. A. Printed Multi-Layer Superstructures of Aligned Single-Walled Carbon Nanotubes for Electronic Applications. *Nano Lett.* **2007**, *7*, 3343–3348.
11. Kocabas, C.; Dunham, S.; Cao, Q.; Cimino, K.; Ho, X.; Kim, H.-S.; Dawson, D.; Payne, J.; Stuenkel, M.; Zhang, H.; *et al.* High-Frequency Performance of Submicrometer Transitions That Use Aligned Arrays of Single-Walled Carbon Nanotubes. *Nano Lett.* **2009**, *9*, 1937–1943.
12. Ishikawa, F. N.; Chang, H.-K.; Ryu, K.; Chen, P.-C.; Badmaev, A.; De Arco, L. G.; Shen, G.; Zhou, C. Transparent Electronics Based on Transfer Printed Aligned Carbon Nanotubes on Rigid and Flexible Substrates. *ACS Nano* **2009**, *3*, 73–79.
13. Murakami, Y.; Chiashi, S.; Miyauchi, Y.; Hu, M. H.; Ogura, M.; Okubo, T.; Maruyama, S. Growth of Vertically Aligned Single-Walled Carbon Nanotubes on Quartz Substrates and Their Optical Anisotropy. *Chem. Phys. Lett.* **2004**, *385*, 298–303.
14. Maruyama, S.; Einarsson, E.; Murakami, Y.; Edamura, T. Growth Process of Vertically Aligned Single-Walled Carbon Nanotubes. *Chem. Phys. Lett.* **2005**, *403*, 320–323.
15. Hata, K.; Futaba, D. N.; Mizuno, K.; Namai, T.; Yumura, M.; Iijima, S. Water-Assisted Highly Efficient Synthesis of Impurity-Free Single-Walled Carbon Nanotubes. *Science* **2004**, *306*, 1362–1364.
16. Futaba, D. N.; Hata, K.; Yamada, T.; Mizuno, K.; Yumura, M.; Iijima, S. Kinetics of Single-Walled Carbon Nanotube Synthesis Revealed by a Time-Evolution Analysis. *Phys. Rev. Lett.* **2005**, *95*, 056104.
17. Zhao, B.; Futaba, D. N.; Yasuda, S.; Akoshima, M.; Yamada, T.; Hata, K. Exploring Advantages of Diverse Carbon Nanotube Forests with Tailored Structures Synthesized by Supergrowth from Engineered Catalysts. *ACS Nano* **2009**, *3*, 108–114.
18. Xiao, L.; Chen, Z.; Feng, C.; Liu, L.; Bai, Z.-Q.; Wang, Y.; Qian, L.; Zhang, Y.; Li, Q.; Jiang, K.; *et al.* Flexible, Strechable, Transparent Carbon Nanotube Thin-Film Loudspeakers. *Nano Lett.* **2008**, *8*, 4539–4545.
19. Liu, P.; Liu, L.; Wei, Y.; Liu, K.; Chen, Z.; Jiang, K.; Li, Q.; Fan, S. *Adv. Mater.* DOI: 10.1002/adma.200900473.
20. Zhang, L.; Feng, C.; Chen, Z.; Liu, L.; Jiang, K. L.; Li, Q. Q.; Fan, S. S. Superaligned Carbon Nanotube Grid for High Resolution Transmission Electron Microscopy of Nanomaterials. *Nano Lett.* **2008**, *8*, 2564–2569.
21. Ren, L.; Pint, C. L.; Booshehri, L. G.; Rice, W. D.; Wang, X.; Hilton, D. J.; Takeya, K.; Kawayama, I.; Tonouchi, M.; Hauge, R. H.; *et al.* Carbon Nanotube Terahertz Polarizer. *Nano Lett.* **2009**, *9*, 2610–2613.
22. Doorn, S. K.; Araujo, P. T.; Hata, K.; Jorio, A. Excitons and Exciton−Phonon Coupling in Metallic Single-Walled Carbon Nanotubes: Resonance Raman Spectroscopy. *Phys. Rev. B* **2008**, *78*, 165408.
23. Majumder, M.; Chopra, N.; Andrews, R.; Hinds, B. J. Nanoscale Hydrodynamics: Enhanced Flow in Carbon Nanotubes. *Nature* **2005**, *438*, 44.
24. Qu, L.; Du, F.; Dai, L. Preferential Synthesis of Semiconducting Vertically Aligned Single-Walled Carbon Nanotubes for Direct Use in FETs. *Nano Lett.* **2008**, *8*, 2682–2687.
25. Mukai, K.; Asaka, K.; Sugino, T.; Kiyohora, K.; Takeuchi, I.; Terasawo, N.; Futaba, D. N.; Hata, K.; Fukushima, T.; Aida, T. Highly Conductive Sheets from Millimeter-Long Single-Walled Carbon Nanotubes and Ionic Liquids: Application to Fast-Moving, Low-Voltage Electromechanical Actuators Operable in Air. *Adv. Mater.* **2009**, *21*, 1582–1585.
26. Zhang, Q.; Zhao, M.; Cao, A.; Qian, W.; Lu, Y.; Wei, F. Energy-Absorbing Hybrid Composites Based on Alternate Carbon Nanotube and Inorganic Layers. *Adv. Mater.* **2009**, *21*, 2876–2880.
27. Xu, Y.; Flor, E.; Kim, M. J.; Hamadani, B.; Schmidt, H.; Smalley, R. E.; Hauge, R. H. Vertical Array Growth of Small Diameter Single-Wall Carbon Nanotubes. *J. Am. Chem. Soc.* **2006**, *128*, 6560–6561.
28. Pint, C. L.; Kim, S. M.; Stach, E. A.; Hauge, R. H. Rapid and Scalable Reduction of Dense Surface-Supported Metal-Oxide Catalyst with Hydrazine Vapor. *ACS Nano* **2009**, *3*, 1897–1905.
29. Pint, C. L.; Pheasant, S. T.; Coulter, K.; Pasquali, M.; Schmidt, H. K.; Hauge, R. H. Synthesis of High Aspect-Ratio Carbon Nanotube "Flying Carpets" from Nanostructured Flake Substrates. *Nano Lett.* **2008**, *8*, 1879–1883.
30. Pint, C. L.; Nicholas, N.; Pheasant, S. T.; Duque, J. G.; Parra-Vasquez, A. N. G.; Eres, G.; Pasquali, M.; Hauge, R. H. Temperature and Gas Pressure Effects in Vertically Aligned Carbon Nanotube Growth from Fe−Mo Catalyst. *J. Phys. Chem. C* **2008**, *112*, 14041–14051.

31. Pint, C. L.; Pheasant, S. T.; Parra-Vasquez, A. N. G.; Horton, C. C.; Xu, Y.; Hauge, R. H. Investigation of Optimal Parameters for Oxide-Assisted Growth of Vertically Aligned Single-Walled Carbon Nanotubes. *J. Phys. Chem. C* **2009**, *113*, 4125–4133.
32. Pint, C. L.; Alvarez, N. T.; Hauge, R. H. Odako Growth of Dense Arrays of Single-Walled Carbon Nanotubes Attached to Carbon Surfaces. *Nano Res.* **2009**, *2*, 526–534.
33. Pint, C. L.; Xu, Y.; Pasquali, M.; Hauge, R. H. Formation of Highly Dense Aligned Ribbons and Transparent Films of Single-Walled Carbon Nanotubes Directly From Carpets. *ACS Nano* **2008**, *2*, 1871–1878.
34. Tsyboulski, D. A.; Bachilo, S. M.; Weisman, R. B. Versatile Visualization of Individual Single-Walled Carbon Nanotubes with Near-Infrared Fluorescence Microscopy. *Nano Lett.* **2005**, *5*, 975–979.
35. Ge, L.; Sethi, S.; Ci, L.; Ajayan, P. M.; Dhinojwala, A. Carbon Nanotube-Based Synthetic Gecko Tapes. *Proc. Natl. Acad. Sci. U.S.A.* **2007**, *104*, 10792–10795.
36. Sethi, S.; Ge, L.; Ci, L.; Ajayan, P. M.; Dhinojwala, A. Gecko-Inspired Carbon Nanotube-Based Self-Cleaning Adhesives. *Nano Lett.* **2008**, *8*, 822–825.
37. Amama, P. B.; Pint, C. L.; McJilton, L.; Kim, S. M.; Stach, E. A.; Murray, P. T.; Hauge, R H.; Maruyama, B. Role of Water in Super Growth of Single-Walled Carbon Nanotube Carpets. *Nano Lett.* **2009**, *9*, 44–49.
38. Pint, C. L.; Nicholas, N.; Duque, J. G.; Parra-Vasquez, A. N. G.; Pasquali, M.; Hauge, R. H. Recycling Ultrathin Catalyst Layers for Multiple Single-Walled Carbon Nanotube Array Regrowth Cycles and Selectivity in Catalyst Activation. *Chem. Mater.* **2009**, *21*, 1550–1556.
39. Im, J.; Lee, I.-H.; Lee, B. H.; Kim, B.; Park, J.; Yu, W.; Kim, U. J.; Lee, Y. H.; Seong, M.-J.; Lee, E. H.; *et al.* Direct Printing of Aligned Carbon Nanotube Patterns for High-Performance Thin Film Devices. *Appl. Phys. Lett.* **2009**, *94*, 053109.
40. Tawfick, S.; O'Brien, K.; Hart, A. J. *Small* **2009**, *94*, 2467–2473.
41. Kazaoui, S.; Minami, N.; Jacquemin, R.; Kataura, H.; Achiba, Y. Amphoteric Doping of Single-Wall Carbon Nanotube Thin Films as Probed by Optical Absorption Spectroscopy. *Phys. Rev. B* **1999**, *60*, 13339.
42. Dresselhaus, M. S.; Dresselhaus, G.; Saito, R.; Jorio, A. Raman Spectroscopy of Carbon Nanotubes. *Phys. Rep.* **2005**, *409*, 47–99.
43. O'Connell, M. J.; Sivaram, S.; Doorn, S. K. Near-Infrared Resonance Raman Excitation Profile Studies of Single-Walled Carbon Nanotube Intertube Interactions; A Direct Comparison of Bundled and Individually Dispersed HiPco Nanotubes. *Phys. Rev. B* **2004**, *69*, 235415.
44. O'Connell, M. J.; Bachilo, S. M.; Huffman, C. B.; Moore, V. C.; Strano, M. S.; Haroz, E. H.; Rialon, K. L.; Boul, P. J.; Noon, W. H.; Kittrell, C.; *et al.* Band Gap Fluorescence From Individual Single-Walled Carbon Nanotubes. *Science* **2002**, *297*, 593–596.
45. Bachilo, S. M.; Strano, M. S.; Kittrell, C.; Hauge, R. H.; Smalley, R. E.; Weisman, R. B. Structure-Assigned Optical Spectra of Single-Walled Carbon Nanotubes. *Science* **2002**, *298*, 2361–2366.
46. Itkis, M. E.; Niyogi, S.; Meng, M. E.; Hamon, M. A.; Hu, H.; Haddon, R. C. Spectroscopic Study of the Fermi Level Electronic Structure of Single-Walled Carbon Nanotubes. *Nano Lett.* **2002**, *2*, 155–159.
47. Ugawa, A.; Rinzler, A. G.; Tanner, D. B. Far-Infrared Gaps in Single-Wall Carbon Nanotubes. *Phys. Rev. B* **1999**, *60*, R11305.
48. Ugawa, A.; Hwang, J.; Gommans, H.; Tashiro, H.; Rinzler, A.; Tanner, D. Far-Infrared to Visible Optical Conductivity of Single-Wall Carbon Nanotubes. *Curr. Appl. Phys.* **2001**, *1*, 45–49.
49. Akima, N.; Isawa, Y.; Brown, S.; Barbour, A. M.; Cao, J.; Musfeldt, J. L.; Matsui, H.; Toyota, N.; Shiraishi, M.; Shimoda, H.; *et al.* Strong Anisotropy in the Far-Infrared Absorption Spectra of Stretch-Aligned Single-Walled Carbon Nanotubes. *Adv. Mater.* **2006**, *18*, 1166–1169.
50. Ren, L.;*et al.* Unpublished results.
51. Niyogi, S.; Hamon, M. A.; Hu, H.; Zhao, B.; Bhowmik, P.; Sen, R.; Itkis, M. E.; Haddon, R. C. Chemistry of Single-Walled Carbon Nanotubes. *Acc. Chem. Res.* **2002**, *35*, 1105–1113.
52. Odom, T. W.; Huang, J.-L.; Kim, P.; Lieber, C. M. Structure and Electronic Properties of Carbon Nanotubes. *J. Phys. Chem. B* **2000**, *104*, 2794–2809.
53. Perebeinos, V.; Tersoff, J.; Avouris, P. Scaling of Excitons in Carbon Nanotubes. *Phys. Rev. Lett.* **2004**, *92*, 257402.
54. Dukovic, G.; Wang, F.; Song, D.; Sfeir, M. Y.; Heinz, T. F.; Brus, L. E. Structural Dependence of Excitonic Optical Transitions and Band-Gap Energies in Carbon Nanotubes. *Nano Lett.* **2005**, *5*, 2314–2318.
55. Kane, C. L.; Mele, E. J. Ratio Problem in Single Carbon Nanotube Fluorescence Spectroscopy. *Phys. Rev. Lett.* **2003**, *90*, 207401.
56. Kane, C. L.; Mele, E. J. Electron Interactions and Scaling Relations for Optical Excitations in Carbon Nanotubes. *Phys. Rev. Lett.* **2004**, *93*, 197402.
57. Jorio, A.; Fantini, C.; Pimenta, M. A.; Capaz, R. B.; Samsonidze, Ge. G.; Dresselhaus, G.; Dresselhaus, M. S.; Jiang, J.; Kobayashi, N.; Gruneis, A.; *et al.* Resonance Raman Spectroscopy (*n*,*m*)-Dependent Effects in Small-Diameter Single-Wall Carbon Nanotubes. *Phys. Rev. B* **2005**, *71*, 075401.
58. Capaz, R. B.; Spataru, C. D.; Ismail-Beigi, S.; Louie, S. G. Diameter and Chirality Dependence of Exciton Properties in Carbon Nanotubes. *Phys. Rev. B* **2006**, *74*, 121401.
59. Capaz, R. B.; Spataru, C. D.; Ismail-Beigi, S.; Louie, S. G. Excitons in Carbon Nanotubes: Diameter and Chirality Trends. *Phys. Status Solidi B* **2007**, *244*, 4016–4020.
60. Maultzsch, J.; Pomraenke, R.; Reich, S.; Chang, E.; Prezzi, D.; Ruini, A.; Molinari, E.; Strano, M. S.; Thomsen, C.; Lienau, C. Exciton Binding Energies in Carbon Nanotubes from Two-Photon Photoluminescence. *Phys. Rev. B* **2005**, *72*, 241402.
61. Weisman, R. B.; Bachilo, S. M. Dependence of Optical Transition Energies on Structure for Single-Walled Carbon Nanotubes in Aqueous Suspension: An Emprical Kataura Plot. *Nano Lett.* **2003**, *3*, 1235–1238.
62. Pint, C. L.; Xu, Y.; Morosan, E.; Hauge, R. H. Alignment Dependence of One-Dimensional Electronic Hopping Transport Observed in Films of Highly Aligned, Ultralong Single-Walled Carbon Nanotubes. *Appl. Phys. Lett.* **2009**, *94*, 182107.
63. O'Connell, M. J.; Eibergen, E. E.; Doorn, S. K. Chiral Selectivity in the Charge-Transfer Bleaching of Single-Walled Carbon Nanotube Spectra. *Nat. Mater.* **2005**, *4*, 412–418.
64. Chen, J.; Hamon, M. A.; Hu, H.; Chen, Y.; Rao, A. M.; Eklund, P. C.; Haddon, R. C. Solution Properties of Single-Walled Carbon Nanotubes. *Science* **1998**, *282*, 95–98.
65. Hu, H.; Zhao, B.; Itkis, M. E.; Haddon, R. C. Nitric Acid Purification of Single-Walled Carbon Nanotubes. *J. Phys. Chem. B* **2003**, *107*, 13838–13842.
66. Itkis, M. E.; Perea, D. E.; Niyogi, S.; Rickard, S. M.; Hamon, M. A.; Hu, H.; Zhao, B.; Haddon, R. C. Purity Evaluation of As-Prepared Carbon Nanotube Soot by Use of Solution-Phase Near-IR Spectroscopy. *Nano Lett.* **2003**, *3*, 309–314.
67. Araujo, P. T.; Maciel, M. O.; Pesce, P. B. C.; Pimenta, M. A.; Doorn, S. K.; Qian, H.; Hartschuh, A.; Steiner, M.; Grigorian, L.; Hata, K.; *et al.* Nature of the Constant Factor in the Relation between Radial Breathing Mode Frequency and Tube Diameter for Single-Wall Carbon Nanotubes. *Phys. Rev. B* **2008**, *77*, 241403.
68. Duesberg, G. S.; Loa, I.; Burghard, M.; Syassen, K.; Roth, S. Polarized Raman Spectroscopy on Isolated Single-Wall Carbon Nanotubes. *Phys. Rev. Lett.* **2000**, *85*, 5436.
69. Murakami, Y.; Chiashi, S.; Einarsson, E.; Maruyama, S. Polarization Dependence of Resonant Raman Scattering from Vertically Aligned Single-Walled Carbon Nanotube Films. *Phys. Rev. B* **2005**, *71*, 085403.
70. Fagan, J. A.; Simpson, J. R.; Landi, B. J.; Richter, L. J.; Mandelbaum, I.; Bajpai, V.; Ho, D. L.; Raffaelle, R.; Hight Walker, A. H.; Bauer, B. J.; *et al.* Dielectric Response of Aligned Semiconducting Single-Wall Carbon Nanotubes. *Phys. Rev. Lett.* **2007**, *98*, 147402.

71. Murakami, Y.; Einarsson, E.; Edamura, T.; Maruyama, S. Polarization Dependence of the Optical Absorption of Single-Walled Carbon Nanotubes. *Phys. Rev. Lett.* **2005**, *94*, 087402.
72. Murakami, Y.; Einarsson, E.; Edamura, T.; Maruyama, S. Polarization Dependent Optical Absorption Properties of Single-Walled Carbon Nanotubes and Methodology for the Evaluation of Their Morphology. *Carbon* **2005**, *43*, 2664–2676.
73. Finnie, P.; Lefebvre, J. Excited Excitonic States in Single-Walled Carbon Nanotubes. *Nano Lett.* **2008**, *8*, 1890–1895.
74. Jorio, A.; Pimenta, M. A.; Souza Filho, A. G.; Samsonidze, Ge. G.; Swan, A. K.; Unlu, M. S.; Goldberg, B. B.; Saito, R.; Dresselhaus, G.; Dresselhaus, M. S. Resonance Raman Spectra of Carbon Nanotubes by Cross-Polarized Light. *Phys. Rev. Lett.* **2003**, *90*, 107403.
75. Gruneis, A.; Saito, R.; Jiang, J.; Samsonidze, Ge. G.; Pimenta, M. A.; Jorio, A.; Souza Filho, A. G.; Dresselhaus, G.; Dresselhaus, M. S. Resonant Raman Spectra of Carbon Nanotube Bundles Observed by Perpendicularly Polarized Light. *Chem. Phys. Lett.* **2004**, *387*, 301–306.
76. Kilina, S.; Tretiak, S.; Doorn, S. K.; Luo, Z. T.; Papadimitrakopoulos, F.; Piryatinski, A.; Saxena, A.; Bishop, A. R. Cross-Polarized Excitons in Carbon Nanotubes. *Proc. Natl. Acad. Sci. U.S.A.* **2008**, *105*, 6797–6802.
77. Wang, H.; Xu, Z.; Eres, G. Order in Vertically Aligned Carbon Nanotube Arrays. *Appl. Phys. Lett.* **2006**, *88*, 213111.
78. Einarsson, E.; Shiozawa, H.; Kramberger, C.; Rummeli, M. H.; Gruneis, A.; Pichler, T.; Maruyama, S. Revealing the Small-Bundle Internal Structure of Vertically Aligned Single-Walled Carbon Nanotube Films. *J. Phys. Chem. C* **2007**, *111*, 17861–17864.
79. Fagan, J. A.; Simpson, J. R.; Bauer, B. J.; Lacerda, S. H. D.; Becker, M. L.; Chun, J.; Migler, K. B.; Walker, A. R. H.; Hobbie, E. K. Length-Dependent Optical Effects in Single-Wall Carbon Nanotubes. *J. Am. Chem. Soc.* **2007**, *129*, 10607–10612.
80. Hwang, J.; Gommans, H. H.; Ugawa, A.; Tashiro, H.; Haggenmueller, R.; Winey, K. I.; Fischer, J. E.; Tanner, D. B.; Rinzler, A. G. Polarized Spectroscopy of Aligned Single-Wall Carbon Nanotubes. *Phys. Rev. B* **2000**, *62*, R13310.
81. Fischer, J. E.; Zhou, W.; Vavro, J.; Llaguno, M. C.; Guthy, C.; Haggenmueller, R.; Casavant, M. J.; Walters, D. E.; Smalley, R. E. Magnetically Aligned Single-Walled Carbon Nanotube Films: Preferred Orientation and Anisotropic Transport Properties. *J. Appl. Phys.* **2003**, *93*, 2157.